Chapter 7

CTAB Complexed Poly(3-thiophene ethanol) - Functionalized MWCNT Nanocomposites for Supercapacitor Application

7.1 Introduction

Establishing new supercapacitor electrode materials is an active area of research for developing energy storage devices.[1-4] Unlike conventional dielectric capacitors, supercapacitors exhibit sound energy density output, a better life cycle, and good energy storage capability. Supercapacitors have widespread applications in electric vehicles, pulse power systems, portable power systems and in renewable energy devices.[5,6] Therefore, developing efficient supercapacitor materials would provide a sustainable storage platform for clean energy production, energy storage, and energy backup systems. High power density, environmental stability, simple operational mechanism, and recyclability are the significant demands for suitable electrode materials in supercapacitor devices.[5-8]

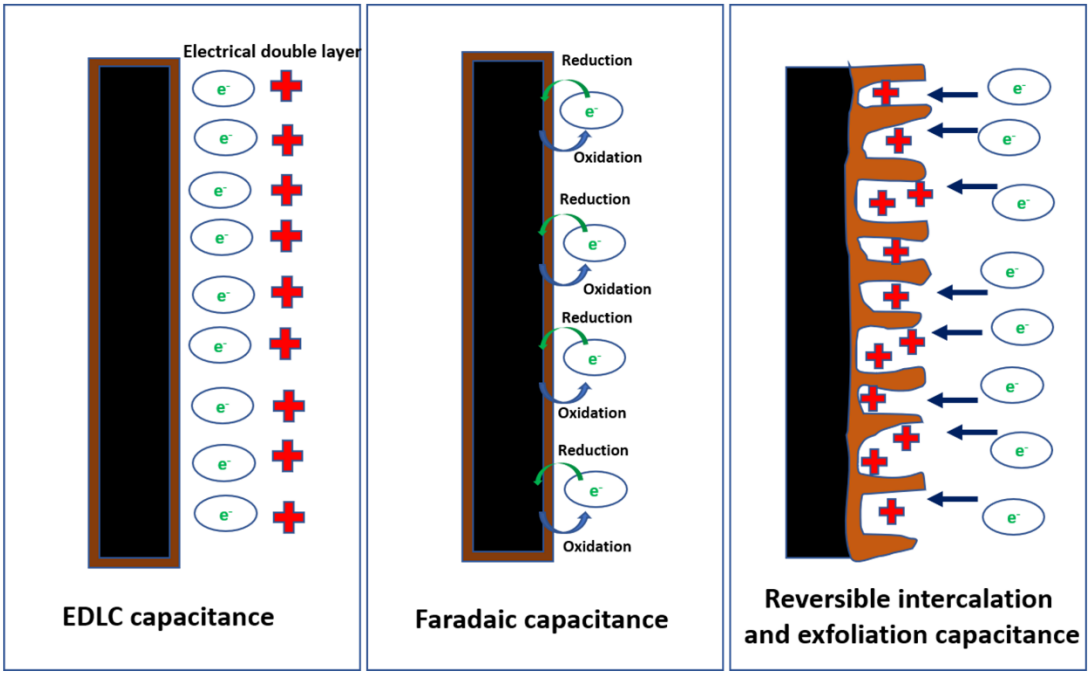

Figure 7.1. *Schematic representations of three types of capacitance based on energy storage mechanism: electrical double layer capacitance (a), reversible faradaic capacitance (b), and reversible intercalation and exfoliation capacitance (c).*

Based on the energy storage mechanism, generally, super capacitance can be classified into three types; electrical double-layer capacitance (EDLC), faradaic capacitance, and intercalation and exfoliation capacitance (see **Figure 7.1.**).[9-10] Selection of supercapacitor electrode material is an important criterion for generating robust, sustainable, and durable devices. Carbonaceous materials such as carbon

nanotubes, graphene, graphite, activated carbon, etc. can act as energy storage materials with an electric double-layer mechanism. Carbon nanotubes are distinguishable with their nano or sub-nanometer pores on their one-dimensional nanotubular surface, which is reasonable for accumulating charges as an electrochemical double-layer assortment.[10-13] Metal oxides, metal hydroxides, and conducting polymers exhibit pseudocapacitive (sequence of faradaic, intercalation, and electrosorption processes) behaviour when used as electrode materials in capacitor applications.[10,12,14-16] Among these pseudocapacitive materials, conducting polymers are attractive for fabricating lightweight, flexible, less toxic, metal-free power storage and delivery systems.[12,14]

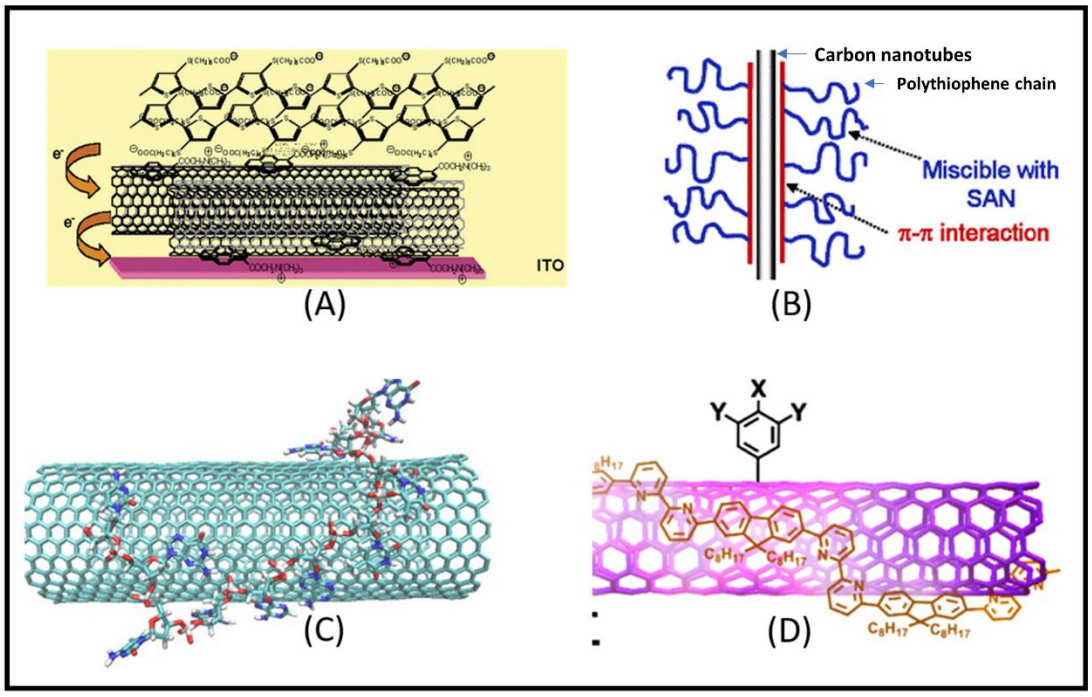

Figure 7.2. *Literature reports of functionalized conducting polymer-carbon nanotube nanocomposites: (A) SWCNT-Pyrene^{+}-polythiophene nanocomposite (adapted from Rahman et al. 2005), (B) polythiophene-graft-poly(methyl methacrylate) (PMMA) as compatibilizer, for poly(styrene-co-acrylonitrile)/ MWCNT nanocomposites (adapted from Kim et al. 2005) (C) Single-Stranded DNA-Single-Walled Carbon Nanotube Hybrid (adapted from Ghosh et al. 2005) and (D) conducting polyfluorene copolymer-Wrapped Carbon Nanotubes (adapted from Berger et al. 2005).*

Polythiophene is an efficient conducting polymer, which is highly desirable for capacitor functions due to its good energy storage capability, electrochemical and environmental stability.[17-19] Enhancement in charge capacity was observed for ultrathin

polythiophenes films as it conserves the large surface area and pore space.[20] Combining electric double-layer capacitive materials with pseudocapacitive polythiophene would be advantageous for high power density and processability.[6,21] Systematic studies on enhancement in capacitive behavior have not much been explored in literature with solid evidence. Supercapacitor electrodes incorporated with conducting polymer may have some obstacles due to poor solubility, lack of surface wettability with electrolyte, and also insufficient conformal coating on other materials.[19,22] Polythiophene derivatives would be more advantageous than unsubstituted polythiophene chains, for attaining solubility in common solvents and to enhance processability. The drawback of substituted polythiophenes instead of unsubstituted polythiophene was that their electrical conductivity and thermal stability might decrease on derivatization. The loss of conductivity and thermal stability can be maintained or enhanced by merging the conducting polymer with other suitable matrices to obtain heterostructural materials such as blends, nanocomposites, nanohybrids, etc.[16,18,23,24] Some of the literature reports of functionalized conducting polymer-carbon nanotube nanocomposites that exhibited superior behaviour than individual components in terms of structure as well as properties is shown in **Figure 7.2.**[25-28]

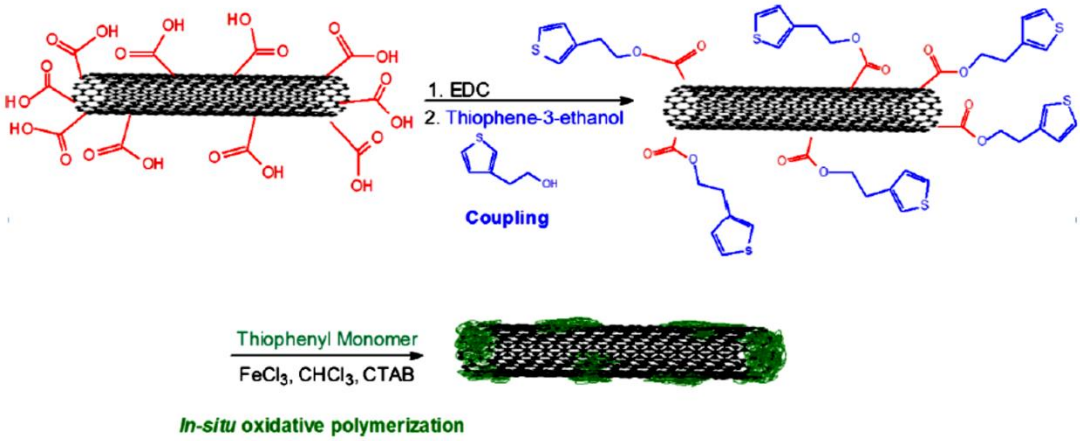

Figure 7.3. *EDC-coupled 3-thiophene ethanol monomer to functionalized MWCNT and subsequent in-situ polymerization to prepare nanocomposites(adapted from Harel et al. 2013).*

The formation of conducting polythiophene nanocomposites with carbon nanotube would be highly promising as supercapacitor electrode materials as it merges electrical double-layer capacitance characteristics of carbon nanotubes with the

pseudocapacitive behavior of polythiophene.[29,30] Generally, the preparation of conducting polymer carbon nanotubes nanocomposites can be carried out by three methods; (i) in-situ polymerization of thiophene/functionalized thiophene monomer in the presence of CNT matrix, (ii) solution blending (ex-situ route) and (iii) melt mixing (ex-situ route).[31-36] In-situ polymerization is more suitable for incorporating insoluble conducting polymers into nanocomposites.[33] On the other hand, solution blending is the strategy for handling soluble forms of conducting polymers toward nanocomposite formation. Soluble forms of conducting polymers attract excellent research interest in nanocomposites formation as the solution blending strategy helps to adopt scalable synthetic procedures with conformally aligned polymer-CNT matrix in nanocomposites.[19,35] Soluble forms of polythiophenes are usually produced by choosing functionalized monomer of thiophene and modifying it into appropriate derivatives.[37] The functionalized monomer 3-thiophene ethanol is a desirable thiophene monomer as the ethanolic group could easily accomplish further reactions with reagents or modify to non-covalent forces.[38-40] There are many reports on the covalent modification of 3-thiophene ethanol for solubility enhancement.[38,39] Harel et al. reported in-situ polymerization of 3-thiophene ethanol monomer to prepare nanocomposite with carboxylic acid functionalized carbon nanotube by directly coupling monomer on CNT surface, without adopting any further modification to the monomer (see **Figure 7.3.**).[41]

In this chapter, we have put forward a facile, simple, and scalable synthetic procedure for poly(3-thiophene ethanol)- functionalized multiwalled carbon nanotube nanocomposites preparation. Poly(3-thiophene ethanol) was initially formed by polymerization of 3-thiophene ethanol monomer using ferric chloride as the oxidant in the presence of AOT surfactant in a chloroform medium. The obtained polymer was then transferred to poly(3-thiophene ethanol)-CTAB complex, which was a soluble complex. Poly(3-thiophene ethanol)-multiwalled carbon nanotubes nanocomposites were prepared by solution blending method of the polymer-CTAB complex with dispersed state of MWCNT-COOH. Polymerization was characterized by FT-IR and MALDI-TOF analysis. Poly(3-thiophene ethanol)-CTAB complex formation was studied with fourier transform infrared spectroscopy and matrix-assisted laser desorption/ionization. Other instrumental analyses such as UV-vis spectroscopy, powder X-ray diffraction, surface morphology, electrical conductivity, and thermal

stability have also been carried out for polymer and polymer-MWCNT-COOH nanocomposites. Capacitance studies of nanocomposites were conducted using cyclic voltammetry and galvanostatic charge-discharge analyses.

7.2. Experimental

7.2.1. Materials and reagents used: 3-Thiophene ethanol, multiwalled carbon nanotubes (MWCNT), AOT, and ferric chloride were purchased from Sigma Aldrich. Cetyl trimethyl ammonium bromide, sodium hydroxide, nitric acid, chloroform, diethyl ether, acetone and deionized water were purchased from Merck chemicals.

7.2.2. Measurements and instruments: Fourier transform-infrared spectra of the samples were recorded by Shimadzu IR Affinity 1 spectrometer using the KBr pellet method. UV-vis spectra of the samples were recorded by Shimadzu UV-Visible spectrophotometer, UV 1800 series, in the range 200-800 nm with HPLC grade chloroform and ethanol. The powder wide-angle X-ray diffraction of the samples was measured using PANALYTICAL, Aeris research with 2θ values ranging from 10 to 80°. FE-SEM images were recorded by ZEISS ΣIGMA^{TM} field emission scanning electron microscope (FE-SEM). MALDI-TOF analysis was conducted with Bruker Autoflex max LRF MALDI-TOF mass spectrometer. Thermogravimetric analysis (TGA) of the samples was measured using Perkin Elmer, Diamond TG/DTA in an inert atmosphere of nitrogen at a heating rate of 20°C/min. The four probe electrical conductivity of the samples was measured using DFP-RM-200 with constant current source Model CCS-01 and DC microvoltmeter. Electrochemical studies were carried out with BioLogic VSP electrochemical workstation unit.

7.2.3 Synthesis of PTE: Monomer (3-thiophene ethanol) (0.5 mL, 4.68 mmol) and surfactant AOT (0.22 g, 0.19 mmol) was dissolved in chloroform (10 mL) and sonicated for 5 min. A dispersed form of $FeCl_3$ (1.06 g, 6.55 mmol) in 5 mL chloroform was added drop by drop to the AOT-thiophene micellar complex mixture and sonicated for 15 min. Subsequently, the reaction mixture was magnetically stirred for 3 h. The polymer thus obtained was filtered and washed using water and acetone. The polymer was then dried in a vacuum oven at 60°C for 3h. Yield: 0.110 g.

7.2.4 Preparation of PTE-CTAB complex: PTE (10 mg) was added into 10 mL dimethyl sulfoxide (DMSO) and taken in a 50 mL RB flask. The mixture was sonicated

for 5 min. Sodium hydroxide (0.0032 g, 0.0792 mmol) was added and magnetically stirred for 5 min. CTAB (0.0289 g, 0.0792 mmol) was then added to the mixture and magnetically stirred for 5 days.

7.2.5 Preparation of PTECNT COOH-10: MWCNT-COOH (0.010 g) dispersed in DMSO (5 mL) was added to the prepared PTE-CTAB complex mixture and sonicated for 15 min. This was then magnetically stirred for 1 h. Double distilled water (100 mL) was then added to it and the resultant product was allowed to precipitate. The powder obtained was then filtered and washed with water. This was then dried in vacuum oven at 80ºC for 3 h. Yield: 0.016 g.

PTECNT-COOH 15 and PTECNT-COOH 20 were prepared by changing the amount of MWCNT-COOH added as 15 mg and 20 mg respectively using same procedure (see **Table 7.1.**).

7.2.6. Electrochemical characterization: Electrochemical measurements were carried out via PTE, MWCNT-COOH and PTECNT-COOH nanocomposites coated on glassy carbon electrode as working electrode, platinum electrode as counter electrode and Ag/AgCl electrode as reference electrode, respectively. Samples were dispersed in ethanol solvent and drop cast into the working electrode without adding any additives or binders. The drop casted samples were dried with air blower. The film coating thus formed was subjected to electrochemical analyses such as cyclic voltammetry and galvanostatic charge-discharge analysis. Cyclic voltammograms were recorded in different scan rates (10 mV/s, 20 mV/s, 50 mV/s, 100 mV/s and 200 mV/s) and using different electrolytes (1M HCl, 1M H_2SO_4, 1M KOH and 1M Na_2SO_4). Galvanostatic charge-discharge studies of PTECNT-COOH 20 with different current densities (0.3 mA/g, 0.6 mA/g and 1.0 mA/g) were carried out in 1M H_2SO_4 electrolyte. The cycling stability of cyclic voltammogram of PTECNT-COOH 20 was also determined for 1000 cycles.

7.3. Results and discussion

7.3.1. Preparation of poly(3-thiophene ethanol) (PTE) and PTECNT-COOH nanocomposites

Synthesis of poly(3-thiophene ethanol) was carried out via oxidative chemical polymerization of 3-thiophene ethanol (TE) monomer using ferric chloride as

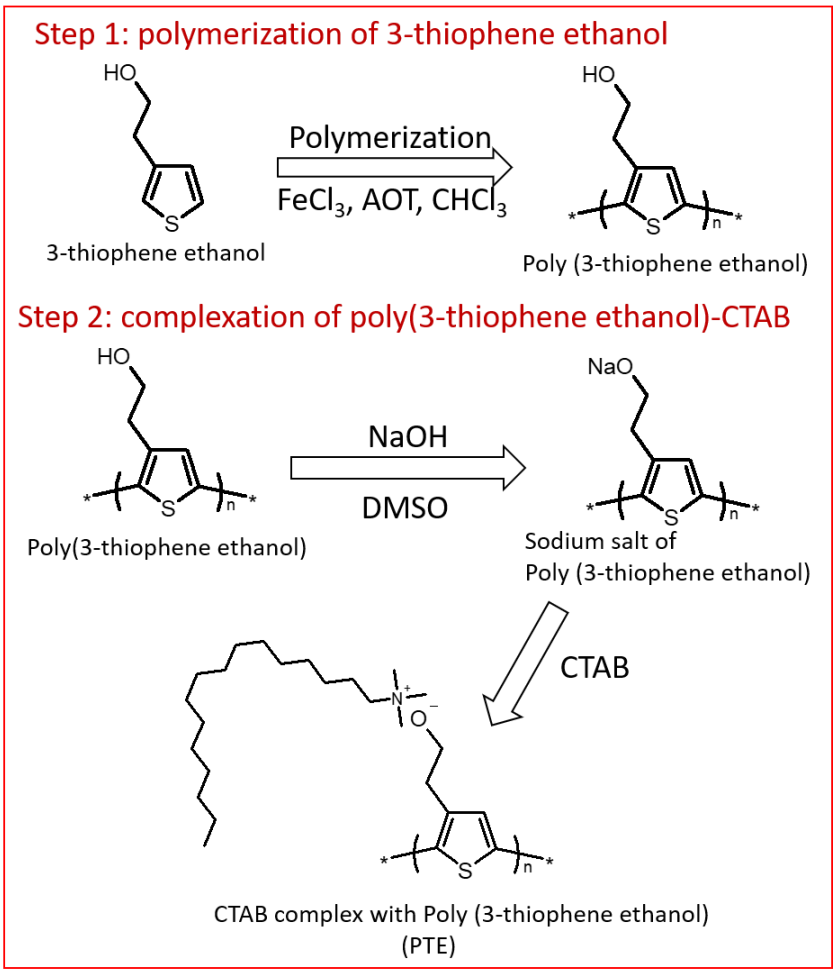

Figure 7.4. *Schematic representation of synthesis of PTE-CTAB complex.*

the oxidant in the presence of surfactant sodium bis (2-ethyl hexyl) sulfosuccinate (AOT) in chloroform medium (see **Figure 7.4.**). The obtained polymer was then sonicated with NaOH in DMSO solvent, resulting in corresponding sodium salt formation. Afterward, the cationic surfactant cetyl trimethyl ammonium bromide (CTAB) was added, sonicated for 15 min, and magnetically stirred for five days. A bright orange-coloured soluble polymer-CTAB complex was thus obtained. A dispersed form of functionalized MWCNT-COOH in DMSO was added slowly to the polymer-CTAB complex. It was then sonicated for 15 min and magnetically stirred for one hour, which resulted in nanocomposite formation (see **Figure 7.5.** and **Table 7.1.**). In the formation of the polymer-CTAB complex, the first stage was the generation of the sodium salt of the ethoxide side chain of thiophene units on the addition of NaOH. The salt form of the polymer then slowly underwent complexation with the cationic

surfactant CTAB on physical agitation. The complex formation of PTE with surfactant occurred due to non-covalent modification on ethoxide side chains of thiophene sub-units in the polymerized form. In this work, soluble polyelectrolyte PTE was prepared using the above mentioned approach which was a less explored way of non-covalent modification.

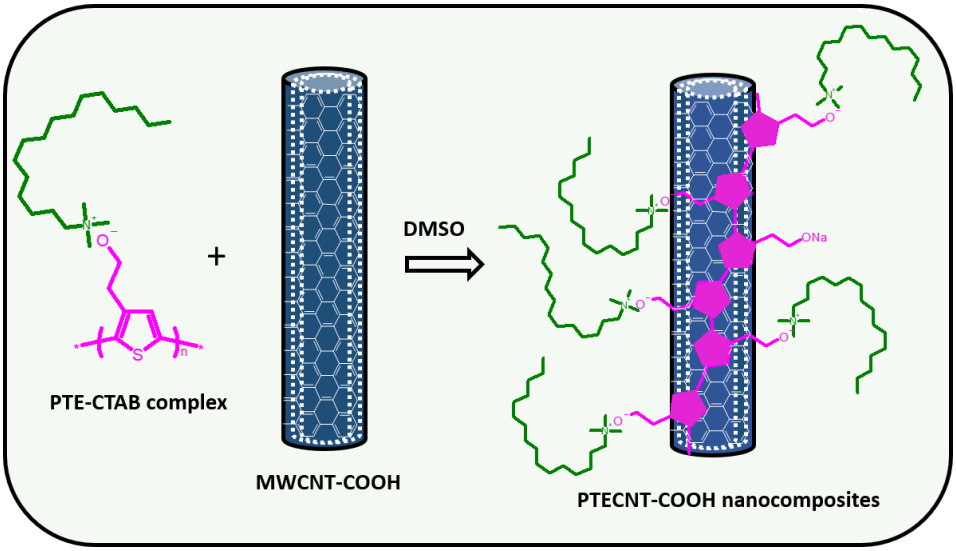

Figure 7.5. *Synthesis of PTECNT-COOH nanocomposites by solution blending method.*

Table 7.1. *PTECNT-COOH samples with the amount of poly(3-thiophene ethanol), CTAB surfactant, MWCNT-COOH used and yield obtained in preparation*

Sample	PTE (mg)	CTAB (mmol)	MWCNT-COOH (mg)	Yield (mg)
PTECNT-COOH 10	10	0.0792	10	16
PTECNT-COOH 15	10	0.0792	15	28
PTECNT-COOH 20	10	0.0792	20	36

7.3.2. Characterization of PTE and PTECNT-COOH nanocomposites

The formation of polymer (PTE), PTE-CTAB complex and nanocomposites (PTECNT-COOH 10, PTECNT-COOH 15 and PTECNT-COOH 20) were characterized using fourier transform infrared spectra (see **Figure 7.6.**). PTE shown characteristic peaks at 813 cm^{-1}, 1022 cm^{-1}, 1722 cm^{-1}, 2852 cm^{-1} and 3000-3700 cm^{-1} indicating C-S stretching vibration, C-O stretching vibration of the ethanolic side chains, stretching vibration of thiophene ring, C-H stretching vibration, and O-H stretching broad vibrational peak respectively.[42,43] Complexation of PTE with CTAB

surfactant was evident from by FTIR analysis. PTE-CTAB complex exhibited peaks at 826 cm^{-1}, 1035 cm^{-1}, 1624 cm^{-1}, 2865 cm^{-1} and 3150-3450 cm^{-1}. For the complex, the peak at 1035 cm^{-1} was found to get intensified compared to PTE. This might be due to the involvement of C-N stretching vibrations present in the CTAB surfactant. A visible shift was observed for IR frequency peak at 1722 cm^{-1} (in PTE) to 1624 cm^{-1} (in PTE-CTAB complex) due to the free stretching vibration of thiophene rings on complexation.[42-45] PTE-CTAB complex exhibited O-H stretching vibration peak arising from the remaining alcoholic groups, which did not participate in complexation. PTECNT-COOH nanocomposites exhibited major peaks at 1035 cm^{-1}, 1524 cm^{-1}, 1624 cm^{-1}, 2852 cm^{-1} and 3000-3650 cm^{-1} attributing to C-O stretching vibration from the side chain, aromatic stretching from carbon nanotubes, thiophene ring stretching vibrations, C-H stretching vibration from 3-thiophene ethanol moiety and O-H stretching vibration from polymer side chain respectively.[42,44,46] Involvement of peaks from the PTE-CTAB complex and MWCNT-COOH in the FT-IR spectra of PTECNT-COOH composites pointed out the effective formation of composites.

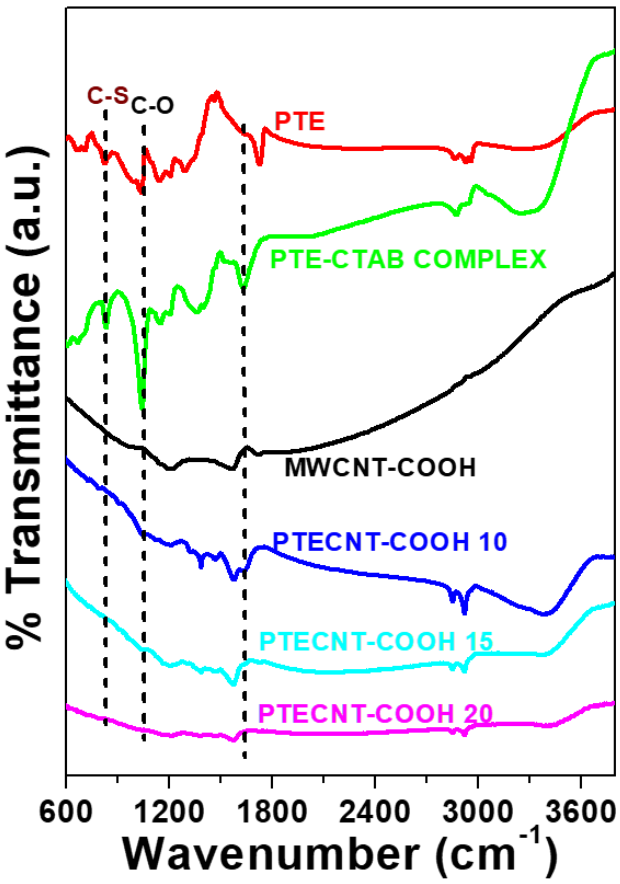

Figure 7.6. *FT-IR spectra of PTE, PTE-CTAB complex, MWCNT-COOH, PTECNT-COOH 10, PTECNT-COOH 15 and PTECNT-COOH 20.*

Solid-state ordering of polymer nanocomposites were analyzed using powder X-ray diffraction. X-ray diffractograms of PTE, PTE-CTAB complex, PTECNT-COOH 10, and PTECNT-COOH 15 were recorded (see **Figure 7.7.**). PTE exhibited a broad, amorphous peak ranging from 2θ value 10-32°.[47] PTE-CTAB complex in which the amorphous peak was changed to partially crystalline with many smaller sharp peaks in it, indicates the formation of short-range ordering in the complexed form of PTE with CTAB. PTECNT-COOH 10 and PTECNT-COOH 15 in which the peak corresponding to (002) plane of multiwalled carbon nanotubes at (2θ=26°) was partially merged with the semi-crystalline peak of PTE-CTAB complex (see **Figure 7.7. inset** also).[48] Presence of diffraction patterns of individual components (PTE and MWCNT-COOH) in X-ray diffractograms of PTECNT-COOH composites confirmed the effective formation of nanocomposites.

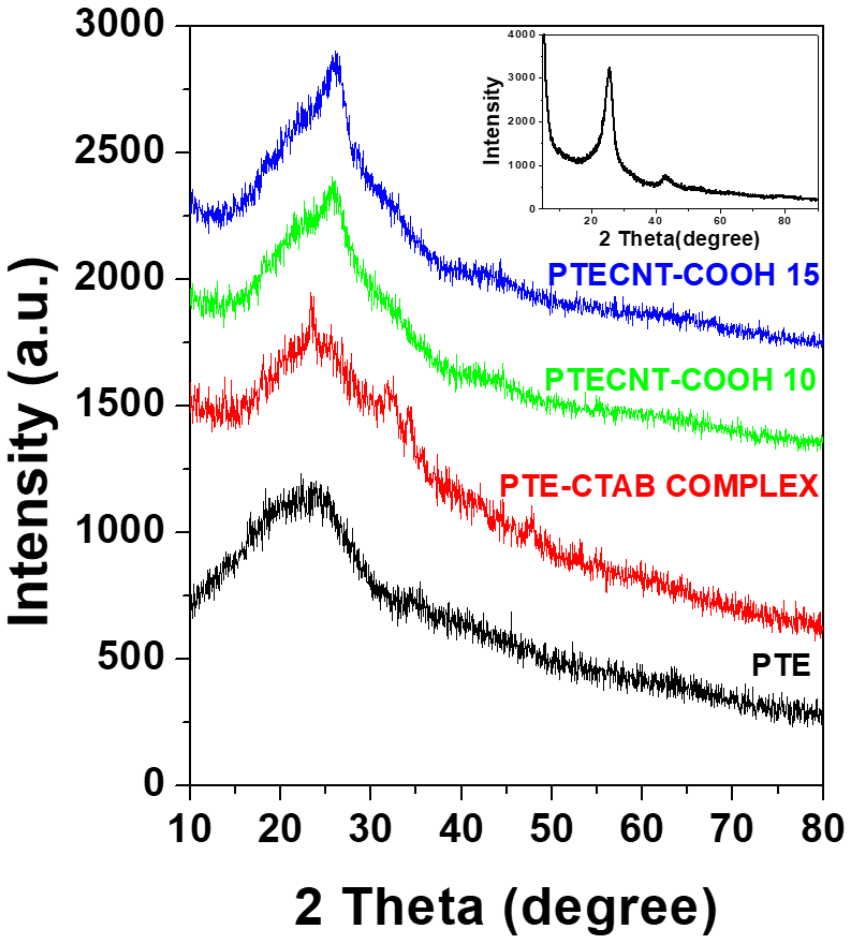

Figure 7.7. *Wide angle X-ray diffractograms of PTE, PTE-CTAB complex, PTECNT-COOH 10, PTECNT-COOH 15 and MWCNT-COOH (inset).*

7.3.3. Morphological and dispersion studies of polymer and PTECNT-COOH nanocomposites

Surface morphologies of PTE, MWCNT-COOH, and PTECNT-COOH nanocomposites were carried out using field emission scanning electron microscopy (see **Figure 7.8.**). Scanning electron microscopic images of PTE appeared as a continuous bulk mass of polymer with some microcavity structures observed in certain areas. Image of one such microcavity is magnified in **Figure 7.8. (inset)** and some other microcavities are marked using yellow dotted circles in **Figure 7.8.** The cavities are shaped nearly as flower bud and these voids might be formed as the effect of AOT surfactant self-assembly during the polymerization. FE-SEM image of MWCNT-COOH has nanotubular morphology with an outer diameter of ~9±3 nm. The morphology of nanocomposites was also found in one-dimensional nanotubes. It was clear from FE-SEM images of composites that no bulk polymer mass was found in the phase-separated form in between the nanotube framework. The outer diameter of nanocomposites with nanotubular structure was observed as ~25±5 nm, which is larger than that of functionalized MWCNT-COOH, indicating the effective wrapping of poly(3-thiophene ethanol)-CTAB complex on the outer surface of carbon nanotubes.

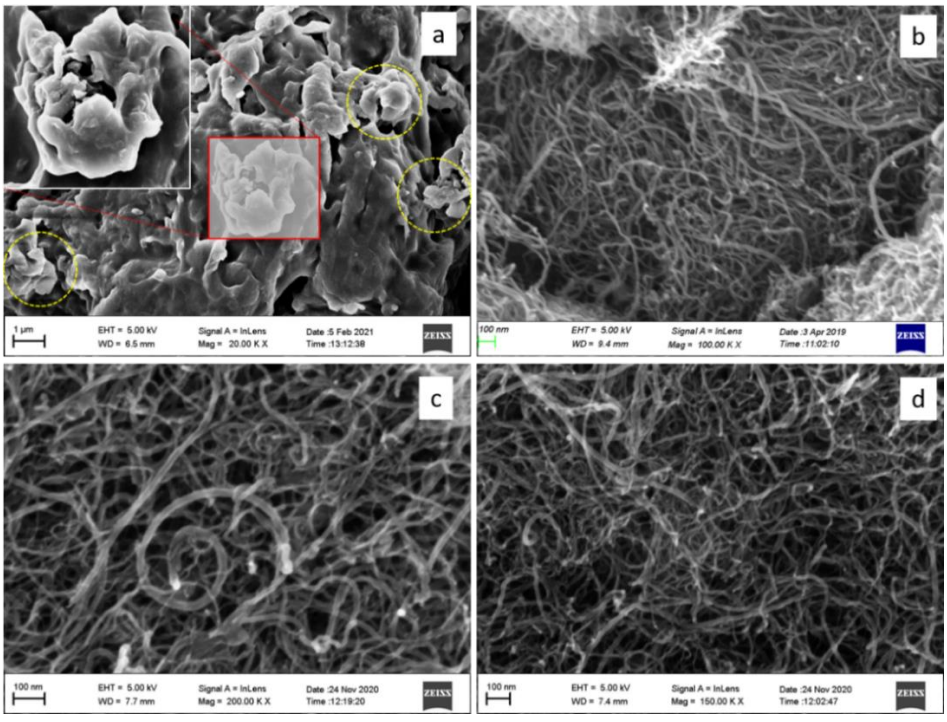

Figure 7.8. *Field emission scanning electron microscopic images of (a) PTE, (b) MWCNT-COOH, (c) PTECNT-COOH 10 and (d) PTECNT-COOH 15.*

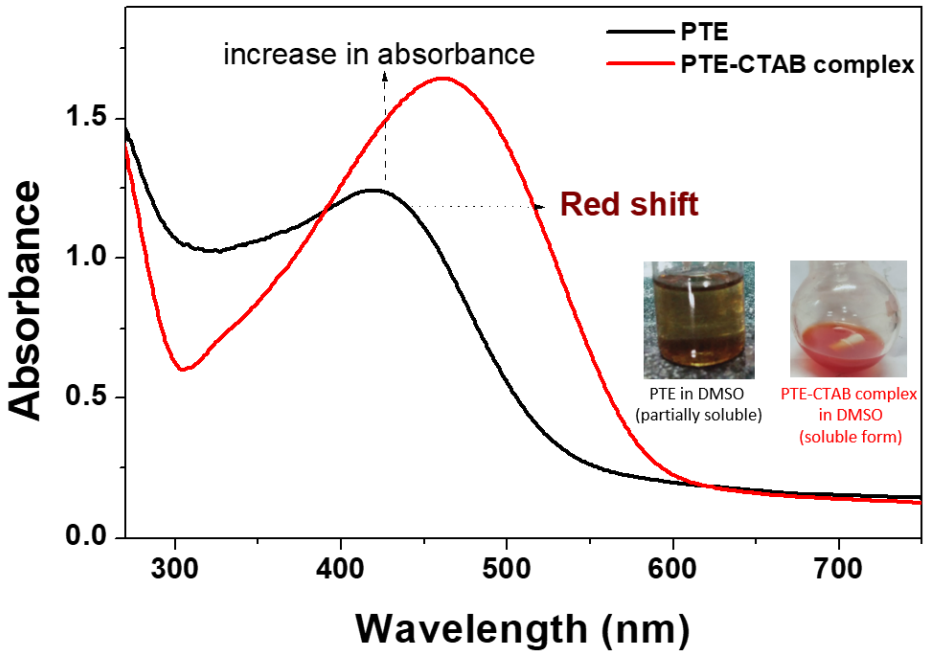

Figure 7.9. *UV-vis absorption spectra of PTE and PTE-CTAB complex.*

The polymer (PTE) exhibited partial solubility in weakly polar organic solvents such as DMSO and NMP (see the photographs in **Figure 7.9.**). Sonication of polymer with NaOH followed by magnetic stirring with cationic surfactant CTAB resulted in the formation of bright orange-coloured complex (PTE-CTAB complex). Absorption studies of polymer PTE and PTE-CTAB complex were carried out with UV-vis spectra (see **Figure 7.9.**). PTE exhibited a peak with an absorption maximum at 420 nm corresponding to polaron-π* transition in polythiophene conjugated chain. For PTE-CTAB complex showed a red shift with broader peak with λ_{max} of 461 nm. The intensity was increased due to the better solubility of the polymer complex in DMSO. The red shift was observed because of the increased extended conjugation of the polythiophene backbone. Complexation of poly(3-thiophene ethanol) with cationic quaternary ammonium surfactant CTAB plausibly released the coiled nature of polymeric chains into a partial rod-like form. This moderate straightening effect might decrease the rotational defects present in PTE chain previously disordered amorphous coiled structure. Insertion of long CTAB chains on polymer creates a sidewise overlap around the polymer, thus restricting the free rotation of polymeric chains to form a coiled structure but promoting partial planarized conformations. As a result, the perturbation in the effective backbone conjugation of polythiophene chains gets decreased and the torsional angles get lessened with a partial straightening effect.[44,49-51] The complex was then subjected to nanocomposites formation with acid functionalized multiwalled

carbon nanotubes (MWCNT-COOH). Nanocomposites thus prepared resulted in stable dispersions in partially polar solvents such as ethanol, DMSO, and NMP (see **Figure 7.10. A**). UV-vis absorption spectra of PTECNT-COOH 10, PTECNT-COOH 15, and PTECNT-COOH 20 were recorded in the solvent ethanol (see **Figure 7.10 B**). The absorption peak arising from the aromatic π-π* transition (λ_{max}= 280 nm) of MWCNT-COOH is in the well-resolved in the UV-vis absorption spectra of nanocomposites. The π-polaron absorption of the polythiophene backbone is observed as an unresolved tail in longer wavelengths continuous with the absorption peak of carbon nanotubes.

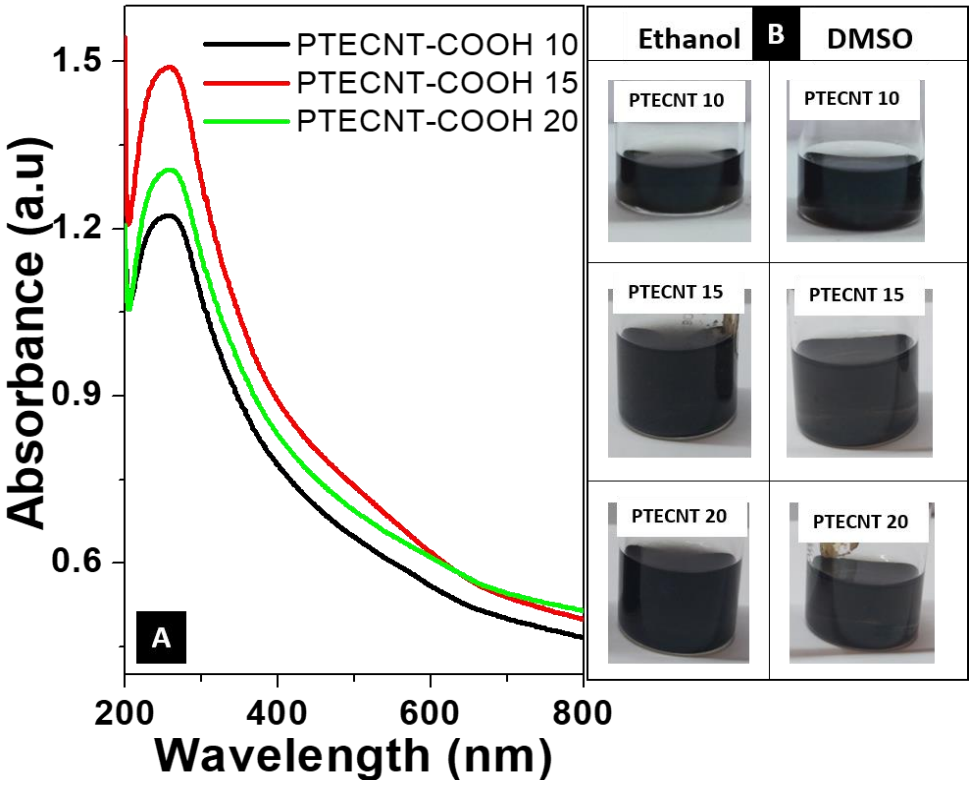

Figure 7.10 *UV-visible spectra of PTECNT-COOH 10, PTECNT-COOH 15 and PTECNT-COOH 20 in ethanol and DMSO (A) and Dispersions of PTECNT-10, PTECNT-15 and PTECNT-20 in ethanol (B).*

Poly(3-thiophene ethanol) complex, effectively wrapped on MWCNT-COOH producing well-defined nanotubular morphology (clearly evident from FE-SEM images of PTECNT-COOH nanocomposites). The average molecular mass of the PTE-CTAB complex obtained from MALDI TOF analysis was 4312.35 g/mol. Preparation of soluble form of poly(3-thiophene ethanol) complex with CTAB surfactant in DMSO helped to utilise the post polymerization preparation of nanocomposite via simple physical blending approach. Sonicated MWCNT-COOH in DMSO acted as stable

dispersion to accommodate complexed polythiophene chains on it via pi-stacking and wraping interaction. Partial uncoiling of PTE chains by complexation eases the association with MWCNT-COOH and their stacked arrangement on carbon nanotubes framework. Thereby polymer got effectively wrapped on carbon nanotubes (the outer radius of PTECNT-COOH was measured to be higher than that of MWCNT-COOH). Pristine carbon nanotubes are characterized by their agglomeration tendency due to their inherent bundling nature. The long hydrophobic alkyl chains orienting outside the tubular framework of nanocomposites restrict interchain aggregation (see **Figure 7.11.**). This might create the well-separated tubular morphology of the nanocomposites as seen in FE-SEM images.

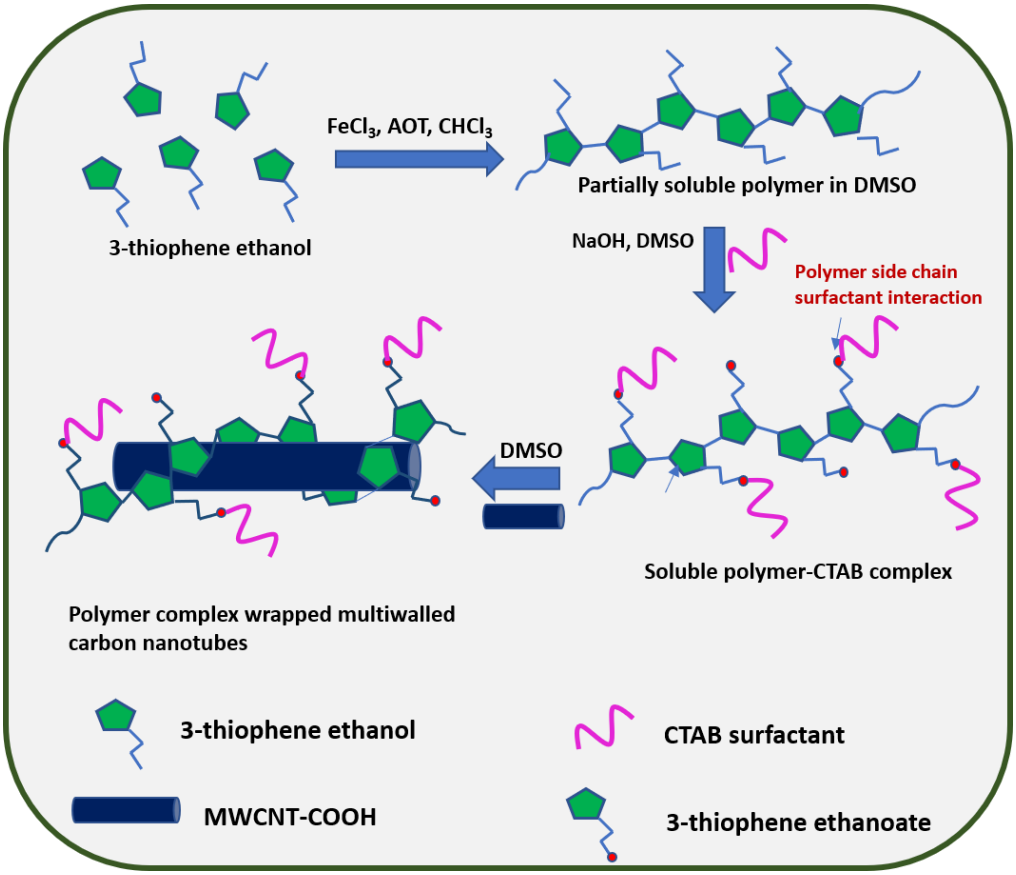

Figure 7.11. *Formation mechanism of PTECNT-COOH nanocomposites.*

7.3.4. Thermal stability and electrical conductivity of PTECNT-COOH nanocomposites

Thermogravimetric analyses were conducted to compare the thermal stability of PTE and PTECNT-COOH nanocomposites prepared (see **Figure 7.12.**). The thermal profile of PTE exhibited two stages of weight loss; the first stage corresponds to the

decomposition of the side chain and the second stage is attributed to polythiophene backbone cleavage.[52] PTECNT-COOH nanocomposites exhibited comparably very high thermal stability than the corresponding polymer. In the initial stage of degradation up to 200°C, PTECNT-COOH composites exhibited only 5% weight loss and PTE showed 10 % weight loss. Further polymer undergo 30%, weight loss upto 300°C as observed in the TGA curve . The thermal profile of PTECNT-COOHs was well above that of PTE, indicating less weight loss occurred in the composites particularly up to 300°C, due to the effective interfacial interaction between polymer and carbon nanotubes. PTECNT-COOH nanocomposites exhibited only 25% weight loss at 700° C indicating the high thermal stability.

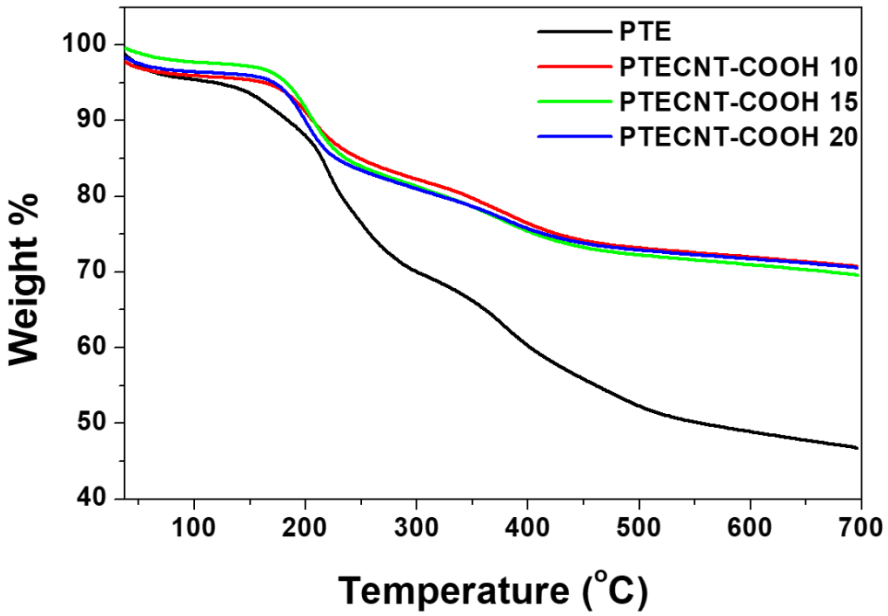

Figure 7.12. *Thermal stability of PTE, PTECNT-COOH 10, PTECNT-COOH 15 and PTECNT-COOH 20.*

The electrical conductivity of PTE, PTECNT-COOH 15, PTECNT-COOH 20 and MWCNT-COOH was measured using four probe electrical conductivity meter (see **Figure 7.13.**). PTE, PTECNT-COOH 15, PTECNT-COOH 20, and MWCNT-COOH exhibited electrical conductivity of 2.21×10^{-8}, 8.33×10^{-1}, 3.31×10^{-1}, and 2.89 S/cm respectively. Poly(3-thiophene ethanol) exhibited very low conductivity compared to unsubstituted polythiophene PT-25 (reported in chapter 2). Incorporating alkyl functional groups with saturated bonds might decrease the conductivity of substituted conducting polymer poly(3-thiophene ethanol). The electrical conductivity of PTECNT-COOH nanocomposites were observed greater than 10^7 orders than that of

PTE. The less conducting PTE composition in the PTECNT-COOH nanocomposites (ie, between 40 % to 50 %), exhibited a hike in conductivity in the polymer-wrapped state on carbon nanotubes. The hike in conductivity might be due to the strong interfacial interaction between polymer and carbon nanotubes through non-bonded interaction between the partially straightened aromatic conjugated backbones of polymer complex and carbon nanotubes.

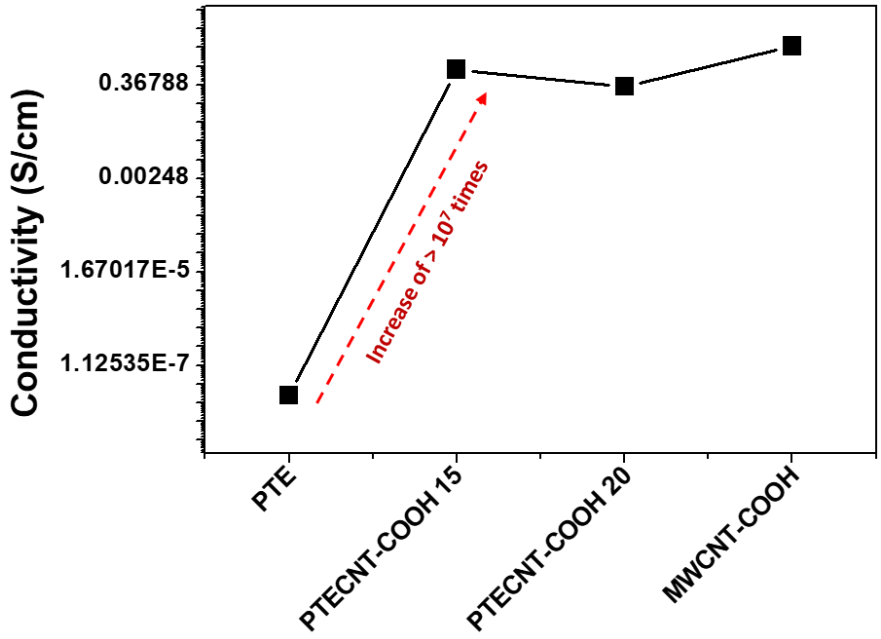

Figure 7.13. *Four probe electrical conductivity of PTE, PTECNT-COOH 15, PTECNT-COOH 20 and MWCNT-COOH.*

7.3.5. Electrochemical characterisation of PTECNT-COOH nanocomposites

The electrochemical performance of PTE, PTECNT-COOH 10, PTECNT-COOH 15, and PTECNT-COOH 20 were analyzed by cyclic voltammetry and galvanostatic-charge-discharge analysis with a three-electrode configuration (see **Figure 7.14.**). The electrochemical cell consists of a modified glassy carbon electrode as working electrode, a platinum electrode as counter electrode and an Ag/AgCl electrode as the reference electrode. The working electrode was prepared by drop casting ethanol solution of samples on glassy carbon electrode and dried with air blow method. A less resolved peak was observed on the cyclic voltammogram of PTE, indicates that both ionic diffusion and the faradaic process influence the electrochemical performance.[49,55,56] PTE exhibited nearly willow-shaped CV curves with a faradaic peak. However, a different quasi-rectangular shape of CV curves of the

PTECNT-COOHs indicated the significant contribution from the MWCNT-COOH component to the electrochemical performance of nanocomposites. Carbon nanotubes exhibit electrical double-layer capacitance from the non-faradaic ionic diffusion process, and corresponding CV curves appear nearly rectangular.[21,53,54] In effect of both faradaic and non-faradaic processes on the PTECNT nanocomposites, the modified glassy carbon electrode was thus found to exhibit pseudocapacitive behaviour.

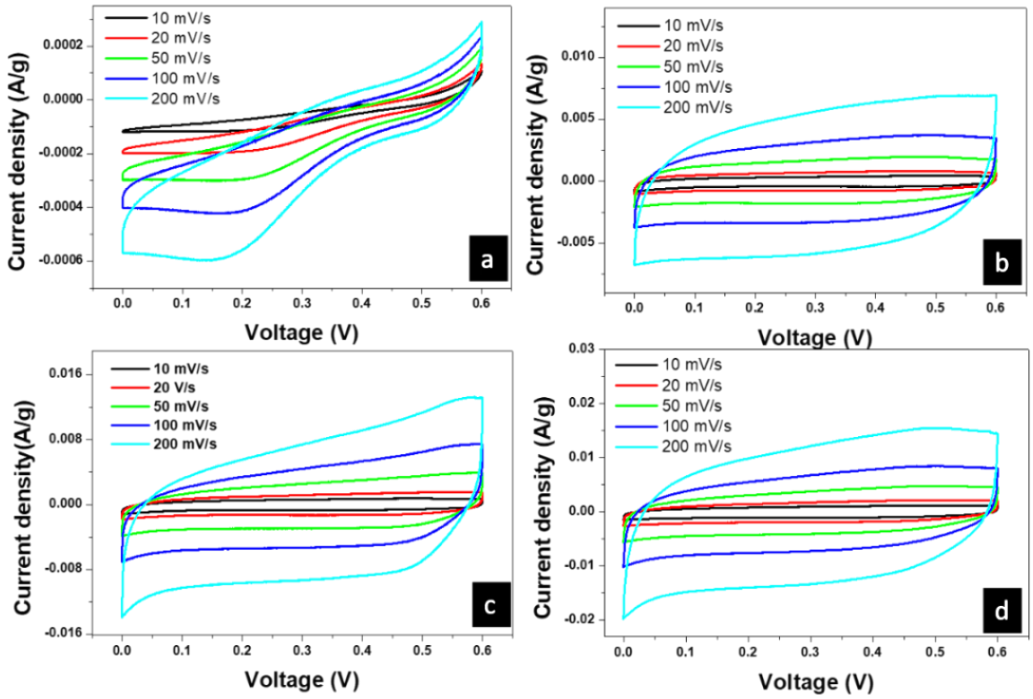

Figure 7.14. *Cyclic voltammogram of PTE (a), PTECNT-COOH 10 (b), PTECNT-COOH 15 (c) and PTECNT-COOH 20 (d) in 1M HCl electrolyte.*

The cyclic voltammetry investigation of PTE, PTECNT-COOH 10, PTECNT-COOH 15, and PTECNT-COOH 20 were carried out in 1 M HCl electrolyte over the potential range of 0 to 0.6 V. The study was carried out for different scan rates, such as 10 mV/s, 20 mV/s, 50 mV/s, 100 mV/s, and 200 mV/s. By comparing the CV curves of PTECNT nanocomposites, the most effective composition was taken as PTECNT-COOH 20 (nanocomposite obtained by adding 20 mg of MWCNT-COOH) which exhibited largest integral area and the highest specific capacitance. Specific capacitance of samples was quantified using the formula

$$C_{sp} = \frac{\int IdV}{2 * m * SR * V \cdot} \cdots\cdots\cdots\cdots\cdots\cdots (1),$$

where 'I' is the current density, 'V' is the potential window, m is the mass of material coated on glassy carbon electrode and 'SR' is the scan rate. ∫IdV is obtained as integral area of CV curves.[23,55] Specific capacitance (C_{sp}) obtained with the samples PTE, PTECNT-COOH 10, PTECNT-COOH 15, and PTECNT-COOH 20 for 10 mV/s were 1.53 F/g, 36.71 F/g, 68.88 F/g, and 90.61 F/g respectively (see **Figure 7.14.**). The specific capacitance of samples was observed to increase with an increase in scan rate,

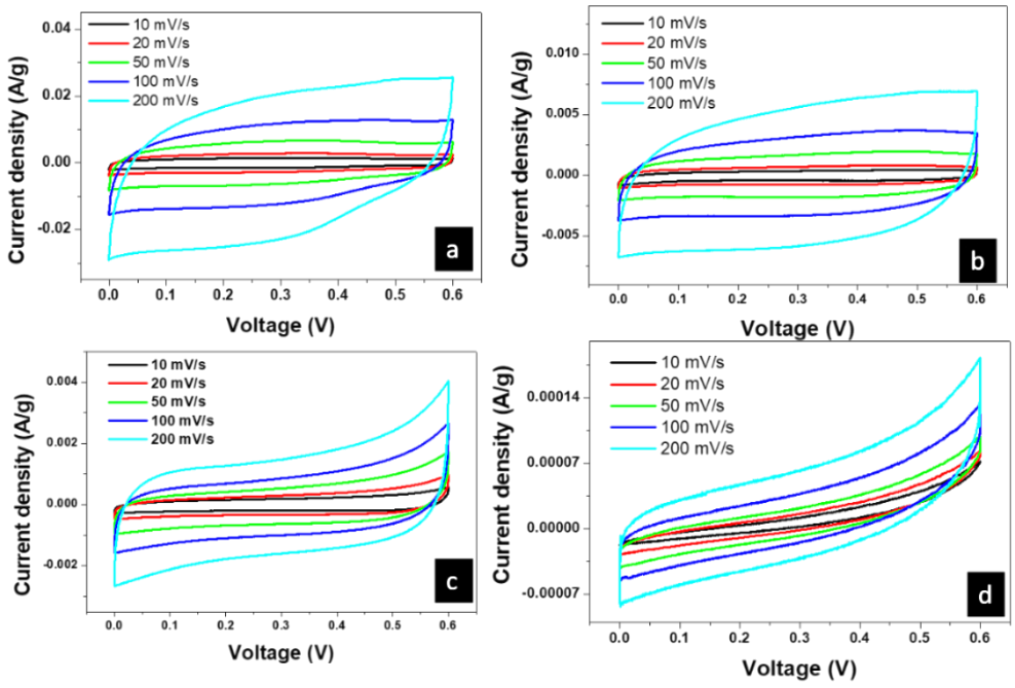

Figure 7.15. *Cyclic voltammogram of PTECNT-COOH 20 for different scan rates in the electrolytes 1M HCl (a), 1M H_2SO_4 (b), 1M KOH (c) and 1M Na_2SO_4 (d).*

indicating the improvement in ionic diffusion. The diffusion kinetics was observed near the diffusion layer and it become more dynamic, thereby giving higher flux towards electrodes and a higher magnitude of the current. Specific capacitance obtained for PTE was found as comparably very small due to less availability of ion-accessible active sites due to its micro-bulk mass structure. However, the nanotubular network structure of PTECNT nanocomposites could provide a sufficient area of active sites to exhibit good electrochemical performance.

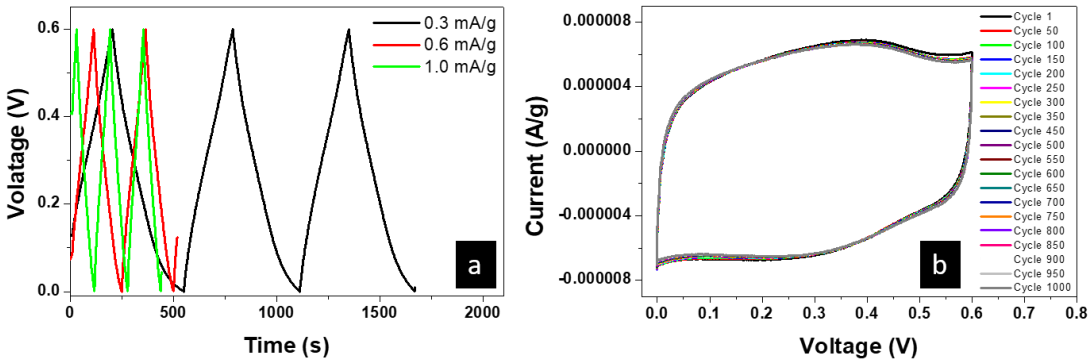

Figure 7.16. *Galvanostatic charge-discharge profile of PTECNT-COOH 20 in 1M H_2SO_4 electrolyte (a) and Cycling stability study (cyclic voltammetry) of PTECNT-COOH 20 in 1M H_2SO_4 electrolyte up to 1000 cycles (b).*

The cyclic voltammograms of PTECNT-COOH 20 were recorded for different electrolyte solutions pocessing different combinations of positive and negative ions. The electrolyte concentrations such as 1M HCl, 1M H_2SO_4, 1M KOH, and 1M Na_2SO_4 were used as aqueous solutions (see **Figure 7.15.**). The highest integral area is obtained for the scan rate 10 mV/s in all the samples and corresponding specific capacitance obtained in 1M HCl, 1M H_2SO_4, 1M KOH, and 1M Na_2SO_4 electrolytes are 90.61 F/g, 123.66 F/g, 13.28 F/g, and 38.13 F/g respectively. Among different aqueous electrolytes used, acidic electrolytes (1M H_2SO_4 and 1 M HCl) have given higher values of specific capacitance. Dibasic H_2SO_4 exhibited the highest electrochemical performance having C_{sp} 123.66 F/g. The charging-discharging analysis of PTECNT-COOH 20 nanocomposites was explored with the GCD (Galvanostatic charge-discharge) characteristic profile at different current densities such as 0.3 mA/g, 0.6 mA/g and 1.0 mA/g (see **Figure 7.16. (a)**). Specific capacitance is measured using the formula,

$$Csp = \frac{It}{m\Delta V} \quad \cdots\cdots\cdots\cdots\cdots\cdots\cdots (2)$$

Where 'I' is the current density, 't' is the discharge time, 'm' is the mass of the sample used and 'ΔV' is the potential window.[23,57] The highest C_{sp} obtained was 180 F/g for 10 mA or 0.3 A/g current density. Comparing the involvement of positive and negative ions to vary specific capacitance of PTECNT-COOH 20, the presence of positive hydrogen ions in electrolytes enhanced the specific capacitance to the higher range. In contrast, other cationic species, such as Na^+ and K^+ had an insignificant impact on

nanocomposite electrochemical performance, which is significant from the difference obtained for C_{sp} values of PTECNT-COOH 20 in two different but same anion-bearing electrolytes 1M H_2SO_4 and 1M Na_2SO_4 . The GCD profile in which deviation of shape from perfect triangular form indicates appreciable pseudo capacitance functioning from conducting polymer wrapping.[57] Comparison of charging and discharging in GCD profiles revealed a higher current density of 1.0 mA/g, at which discharging time increases appreciably than charging time. The difference between charging and discharging time is not appreciable at lower current densities. A longer discharging time observed in PTECNT-COOH 20 nanocomposites indicates the more charge storage capability of the PTECNT-COOH-modified glassy carbon electrode.[7] Other quantitative measurements, such as energy density and power density, were also quantified. Energy density was calculated using the equation,

$$Energy\ density = \frac{CV^2}{8 * 3.6} \quad \cdots\cdots\cdots\cdots\cdots\cdots (2),$$

Where 'C' is the specific capacitance in F/g and 'V' is the potential window in volts. Then power density was also calculated using the equation,

$$Power\ density = \frac{E}{\Delta t} \quad \cdots\cdots\cdots\cdots\cdots\cdots (3),$$

Where E is the energy density and Δt is the time.[57] Energy density was obtained as 1.6 Wh/Kg and power density as 19.19 W/Kg. Both energy and power density met moderately good performance for supercapacitors along with its high specific capacitance of 128 F/g. The electrochemical stability of PTECNT-COOH 20 nanocomposite electrode was analyzed with cyclic voltammetry in the scan rate of 200 mV/s for the continuous 1000 cycles (see **Figure 7.16. (b)**). The specific capacitance of 99 % was found to be retained even after 1000 cycles. Supercapacitors with high cycling stability are challenging to generate the long-term output from the electrode materials.[58,59] Preparation of electrodes by coating as a film without adding additives or binders is another good advantage in a capacitor's economic and efficiency aspects.[60] In essence, we have put forward a facile physical blending approach for thermally stable and conducting nanocomposites preparation. The composite was effectively demonstrated for applying easily fabricated, moderately good capacitive, energy

efficient, competent power generating and a long-lasting supercapacitor (see **Figure 7.17.**).

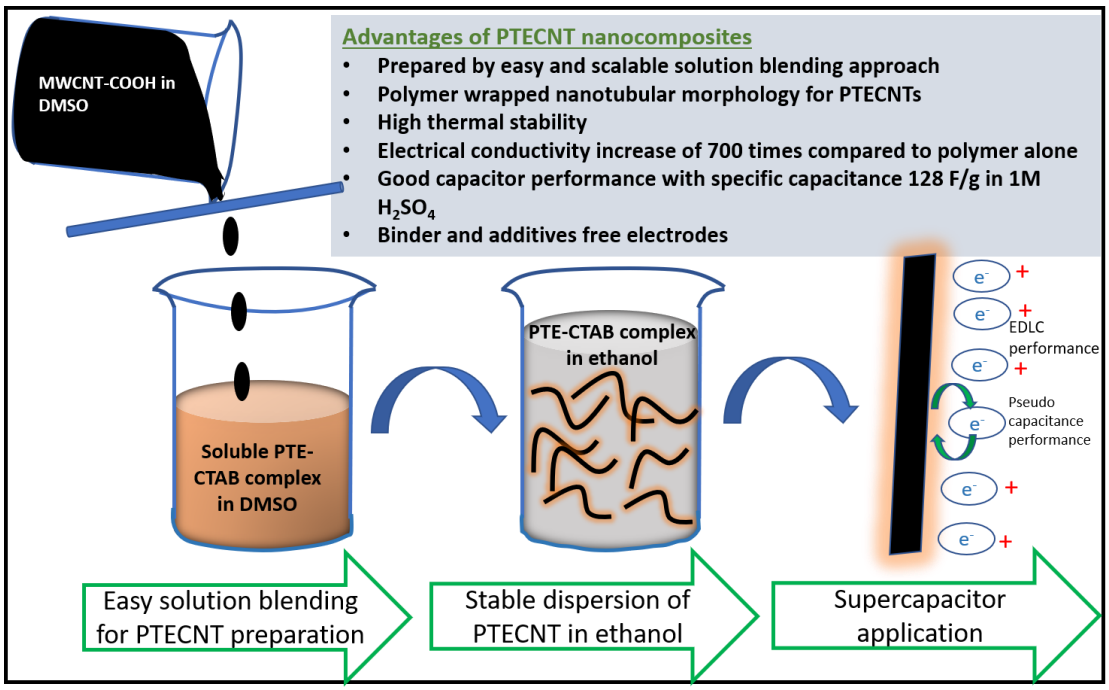

Figure 7.17. *Illustration of advantageous outputs of PTECNT-COOH nanocomposites preparation and its supercapacitor application.*

7.4. Conclusion

Poly(3-thiophene ethanol)-functionalized multiwalled carbon nanotube nanocomposites (PTECNT-COOH) was prepared by scalable and less complicated physical blending route in DMSO solvent. Poly(3-thiophene ethanol) (PTE) was initially prepared by oxidative chemical polymerisation using ferric chloride as an oxidant in the presence of AOT as surfactant in chloroform medium. PTE is then complexed with cationic surfactant cetyl trimethyl ammonium bromide (CTAB) to obtain the solubilized form of the polymer PTE-CTAB complex. FT-IR analysis and powder X-ray diffraction studies confirms the PTECNT-COOH nanocomposites formation. PTE-CTAB complex exhibited an intensified red shift in absorption spectra, indicating the conformational change of the polymer backbone, resulting in efficient conformationaly extended conjugation. PTECNT-COOH composites exhibited stable dispersion in less polar solvents; especially in ethanol, which helped to record UV-vis absorption spectra. Morphological analyses using FE-SEM micrographs gave less agglomerated nanotubular morphology of the nanocomposites. PTECNT-COOH

composites maintained high thermal stability and good electrical conductivity. Additives and binders free preparation of film coating of PTECNT-COOH with green solvent ethanol was achieved for electrochemical characterization. The electrochemical study shows the applicability of PTECNT-COOH nanocomposites as efficient supercapacitor electrode material having a moderately good specific capacitance of 128 F/g with efficient energy density, power output and long-time cycling stability.

References

1. Avasthi, P.; Kumar, A.; Balakrishnan, V. Aligned CNT Forests on Stainless Steel Mesh for Flexible Supercapacitor Electrode with High Capacitance and Power Density. *ACS Appl. Nano Mater.* **2019**, *2* (3), 1484–1495. https://doi.org/10.1021/acsanm.8b02355.
2. Kumar, S.; Saeed, G.; Zhu, L.; Hui, K. N.; Kim, N. H.; Lee, J. H. 0D to 3D Carbon-Based Networks Combined with Pseudocapacitive Electrode Material for High Energy Density Supercapacitor: A Review. *Chem. Eng. J.* **2021**, *403*. https://doi.org/10.1016/j.cej.2020.126352.
3. Han, J.; Wang, S.; Zhu, S.; Huang, C.; Yue, Y.; Mei, C.; Xu, X.; Xia, C. Electrospun Core-Shell Nanofibrous Membranes with Nanocellulose-Stabilized Carbon Nanotubes for Use as High-Performance Flexible Supercapacitor Electrodes with Enhanced Water Resistance, Thermal Stability, and Mechanical Toughness. *ACS Appl. Mater. Interfaces* **2019**, *11* (47), 44624–44635. https://doi.org/10.1021/acsami.9b16458.
4. Yang, Z.; Tian, J.; Yin, Z.; Cui, C.; Qian, W.; Wei, F. Carbon Nanotube- and Graphene-Based Nanomaterials and Applications in High-Voltage Supercapacitor: A Review. *Carbon N. Y.* **2019**, *141*, 467–480. https://doi.org/10.1016/j.carbon.2018.10.010.
5. Aydinli, A.; Yuksel, R.; Unalan, H. E. Vertically Aligned Carbon Nanotube – Polyaniline Nanocomposite Supercapacitor Electrodes. *Int. J. Hydrogen Energy* **2018**, *43* (40), 18617–18625. https://doi.org/10.1016/j.ijhydene.2018.05.126.
6. Saha, S.; Samanta, P.; Murmu, N. C.; Kuila, T. A Review on the Heterostructure Nanomaterials for Supercapacitor Application. *J. Energy Storage* **2018**, *17*, 181–202. https://doi.org/10.1016/j.est.2018.03.006.
7. Dhibar, S.; Bhattacharya, P.; Ghosh, D.; Hatui, G.; Das, C. K. Graphene-Single-Walled Carbon Nanotubes-Poly(3-Methylthiophene) Ternary Nanocomposite for Supercapacitor Electrode Materials. *Ind. Eng. Chem. Res.* **2014**, *53* (33), 13030–13045. https://doi.org/10.1021/ie501407k.
8. Li, Y.; Zhou, M.; Wang, Y.; Pan, Q.; Gong, Q.; Xia, Z.; Li, Y. Remarkably Enhanced Performances of Novel Polythiophene-Grafting-Graphene Oxide Composite via Long Alkoxy Linkage for Supercapacitor Application. *Carbon N. Y.* **2019**, *147*, 519–531. https://doi.org/10.1016/j.carbon.2019.03.030.
9. Ghosh, A.; Lee, Y. H. Carbon-Based Electrochemical Capacitors. *ChemSusChem* **2012**, *5* (3), 480–499. https://doi.org/10.1002/cssc.201100645.
10. Lokhande, P. E.; Chavan, U. S.; Pandey, A. Materials and Fabrication Methods for Electrochemical Supercapacitors: Overview. *Electrochem. Energy Rev.* **2020**, *3* (1), 155–186. https://doi.org/10.1007/s41918-019-00057-z.
11. Li, L.; Hu, Z. A.; An, N.; Yang, Y. Y.; Li, Z. M.; Wu, H. Y. Facile Synthesis of MnO2/CNTs Composite for Supercapacitor Electrodes with Long Cycle Stability. *J. Phys. Chem. C* **2014**, *118* (40), 22865–22872. https://doi.org/10.1021/jp505744p.
12. Yu, G.; Hu, L.; Liu, N.; Wang, H.; Vosgueritchian, M.; Yang, Y.; Cui, Y.; Bao, Z. Enhancing the Supercapacitor Performance of Graphene/MnO2 Nanostructured Electrodes by Conductive Wrapping. *Nano Lett.* **2011**, *11* (10), 4438–4442. https://doi.org/10.1021/nl2026635.

13. Huang, Y.; Wang, B.; Liu, F.; Liu, H.; Wang, S.; Li, Q.; Cheng, J.; Zhang, L. Fabrication of Rambutan-like Activated Carbon Sphere/Carbon Nanotubes and Their Application as Supercapacitors. *Energy and Fuels* **2021**, *35* (9), 8313–8320. https://doi.org/10.1021/acs.energyfuels.1c00189.
14. Bryan, A. M.; Santino, L. M.; Lu, Y.; Acharya, S.; D'Arcy, J. M. Conducting Polymers for Pseudocapacitive Energy Storage. *Chem. Mater.* **2016**, *28* (17), 5989–5998. https://doi.org/10.1021/acs.chemmater.6b01762.
15. Faraji, S.; Ani, F. N. Microwave-Assisted Synthesis of Metal Oxide/Hydroxide Composite Electrodes for High Power Supercapacitors - A Review. *J. Power Sources* **2014**, *263*, 338–360. https://doi.org/10.1016/j.jpowsour.2014.03.144.
16. Kumar, K. S.; Choudhary, N.; Jung, Y.; Thomas, J. Recent Advances in Two-Dimensional Nanomaterials for Supercapacitor Electrode Applications. *ACS Energy Lett.* **2018**, *3* (2), 482–495. https://doi.org/10.1021/acsenergylett.7b01169.
17. So, R. C.; Carreon-Asok, A. C. Molecular Design, Synthetic Strategies, and Applications of Cationic Polythiophenes. *Chem. Rev.* **2019**, *119* (21), 11442–11509. https://doi.org/10.1021/acs.chemrev.8b00773.
18. Kaloni, T. P.; Giesbrecht, P. K.; Schreckenbach, G.; Freund, M. S. Polythiophene: From Fundamental Perspectives to Applications. *Chem. Mater.* **2017**, *29* (24), 10248–10283. https://doi.org/10.1021/acs.chemmater.7b03035.
19. Nejati, S.; Minford, T. E.; Smolin, Y. Y.; Lau, K. K. S. Enhanced Charge Storage of Ultrathin Polythiophene Films within Porous Nanostructures. *ACS Nano* **2014**, *8* (6), 5413–5422. https://doi.org/10.1021/nn500007c.
20. Wang, X.; Zhu, Y.; Liu, Z.; Yuan, Y.; Qiu, L. Ultrathin Polythiophene Films Prepared by Vertical Phase Separation for Highly Stretchable Organic Field-Effect Transistors. *Adv. Electron. Mater.* **2021**, *7* (11). https://doi.org/10.1002/aelm.202100591.
21. Devadas, B.; Imae, T. Effect of Carbon Dots on Conducting Polymers for Energy Storage Applications. *ACS Sustain. Chem. Eng.* **2018**, *6* (1), 127–134. https://doi.org/10.1021/acssuschemeng.7b01858.
22. Hashempour, M.; Vicenzo, A.; Bahdanchyk, M.; Bestetti, M. Parameters Influencing the Capacitive Behavior of Carbon Composite Electrodes: Composition, Morphology, Electrical Conductivity, and Surface Chemistry. *J. Solid State Electrochem.* **2018**, *22* (12), 3895–3911. https://doi.org/10.1007/s10008-018-4095-8.
23. Alvi, F.; Ram, M. K.; Basnayaka, P. A.; Stefanakos, E.; Goswami, Y.; Kumar, A. Graphene-Polyethylenedioxythiophene Conducting Polymer Nanocomposite Based Supercapacitor. *Electrochim. Acta* **2011**, *56* (25), 9406–9412. https://doi.org/10.1016/j.electacta.2011.08.024.
24. Poonam; Sharma, K.; Arora, A.; Tripathi, S. K. Review of Supercapacitors: Materials and Devices. *J. Energy Storage* **2019**, *21*, 801–825. https://doi.org/10.1016/j.est.2019.01.010.
25. Rahman, G. M. A.; Guldi, D. M.; Cagnoli, R.; Mucci, A.; Schenetti, L.; Vaccari, L.; Prato, M. Combining Single Wall Carbon Nanotubes and Photoactive Polymers for Photoconversion. *J. Am. Chem. Soc.* **2005**, *127* (28), 10051–10057. https://doi.org/10.1021/ja050396k.
26. Kim, K. H.; Jo, W. H. Synthesis of Polythiophene-*graft*-PMMA and Its Role as Compatibilizer for Poly(styrene-*co*-acrylonitrile)/MWCNT Nanocomposites, *Macromolecules,* **2007,** *40 (10), 20189*,https://doi.org/10.1021/ma070127.
27. Ghosh, S.; Patel, N.; Chakrabarti, R. Probing the Salt Concentration Dependent Nucelobase Distribution in a Single-Stranded DNA-Single-Walled Carbon Nanotube Hybrid with Molecular Dynamics. *J. Phys. Chem. B* **2016**, *120* (3), 455–466. https://doi.org/10.1021/acs.jpcb.5b12044.
28. Berger, F. J.; Lüttgens, J.; Nowack, T.; Kutsch, T.; Lindenthal, S.; Kistner, L.; Müller, C. C.; Bongartz, L. M.; Lumsargis, V. A.; Zakharko, Y.; Zaumseil, J. Brightening of Long, Polymer-Wrapped Carbon Nanotubes by Sp3 Functionalization in Organic Solvents. *ACS Nano* **2019**, *13* (8), 9259–9269. https://doi.org/10.1021/acsnano.9b03792.

29. Wang, J.; Dai, J.; Yarlagadda, T. Carbon Nanotube-Conducting-Polymer Composite Nanowires. *Langmuir* **2005**, *21* (1), 9–12. https://doi.org/10.1021/la0475977.
30. Lota, K.; Khomenko, V.; Frackowiak, E. Capacitance Properties of Poly(3,4-Ethylenedioxythiophene)/Carbon Nanotubes Composites. *J. Phys. Chem. Solids* **2004**, *65* (2–3), 295–301. https://doi.org/10.1016/j.jpcs.2003.10.051.
31. Zhan, C.; Yu, G.; Lu, Y.; Wang, L.; Wujcik, E.; Wei, S. Conductive Polymer Nanocomposites: A Critical Review of Modern Advanced Devices. *J. Mater. Chem. C* **2017**, *5* (7), 1569–1585. https://doi.org/10.1039/c6tc04269d.
32. Cheung, W.; Chiu, P. L.; Parajuli, R. R.; Ma, Y.; Ali, S. R.; He, H. Fabrication of High Performance Conducting Polymer Nanocomposites for Biosensors and Flexible Electronics: Summary of the Multiple Roles of DNA Dispersed and Functionalized Single Walled Carbon Nanotubes. *J. Mater. Chem.* **2009**, *19* (36), 6465–6480. https://doi.org/10.1039/b823065j.
33. Zhou, K.; He, Y.; Xu, Q.; Zhang, Q.; Zhou, A.; Lu, Z.; Yang, L. K.; Jiang, Y.; Ge, D.; Liu, X. Y.; Bai, H. A Hydrogel of Ultrathin Pure Polyaniline Nanofibers: Oxidant-Templating Preparation and Supercapacitor Application. *ACS Nano* **2018**, *12* (6), 5888–5894. https://doi.org/10.1021/acsnano.8b02055.
34. Tang, C.; Chen, N.; Hu, X. Conducting Polymer Nanocomposites: Recent Developments and Future Prospects. **2017**, 1–44. https://doi.org/10.1007/978-3-319-46458-9_1.
35. Dunlop, M. J.; Bissessur, R. Nanocomposites Based on Graphene Analogous Materials and Conducting Polymers: A Review. *J. Mater. Sci.* **2020**, *55* (16), 6721–6753. https://doi.org/10.1007/s10853-020-04479-9.
36. Yin, S.; Lu, W.; Wu, R.; Fan, W.; Guo, C. Y.; Chen, G. Poly(3,4-Ethylenedioxythiophene)/Te/Single-Walled Carbon Nanotube Composites with High Thermoelectric Performance Promoted by Electropolymerization. *ACS Appl. Mater. Interfaces* **2020**, *12* (3), 3547–3553. https://doi.org/10.1021/acsami.9b17947.
37. Namsheer, K.; Rout, C. S. Conducting Polymers: A Comprehensive Review on Recent Advances in Synthesis, Properties and Applications. *RSC Adv.* **2021**, *11* (10), 5659–5697. https://doi.org/10.1039/d0ra07800j.
38. Tran-Van, F.; Carrier, M.; Chevrot, C. Sulfonated Polythiophene and Poly(3,4-Ethylenedioxythiophene) Derivatives with Cations Exchange Properties. *Synth. Met.* **2004**, *142* (1–3), 251–258. https://doi.org/10.1016/j.synthmet.2003.09.013.
39. Ghosh, R.; Chatterjee, D. P.; Das, S.; Mukhopadhyay, T. K.; Datta, A.; Nandi, A. K. Influence of Hofmeister I- on Tuning Optoelectronic Properties of Ampholytic Polythiophene by Varying PH and Conjugating with RNA. *Langmuir* **2017**, *33* (44), 12739–12749. https://doi.org/10.1021/acs.langmuir.7b03147.
40. Das, S.; Chatterjee, D. P.; Ghosh, R.; Nandi, A. K. Water Soluble Polythiophenes: Preparation and Applications. *RSC Adv.* **2015**, *5* (26), 20160–20177. https://doi.org/10.1039/c4ra16496b.
41. Harel, Y.; Azoubel, S.; Magdassi, S.; Lellouche, J. P. A Dispersability Study on Poly(Thiophen-3-Yl-Acetic Acid) and PEDOT Multi-Walled Carbon Nanotube Composites Using an Analytical Centrifuge. *J. Colloid Interface Sci.* **2013**, *390* (1), 62–69. https://doi.org/10.1016/j.jcis.2012.09.006.
42. Zhao, Q.; Li, Y.; Hu, K.; Guo, X.; Qu, Y.; Li, Z.; Yang, F.; Liu, H.; Qin, C.; Jing, L. Controlled Synthesis of Nitro-Terminated Poly[2-(3-Thienyl)-Ethanol]/g-C3N4Nanosheet Heterojunctions for Efficient Visible-Light Photocatalytic Hydrogen Evolution. *ACS Sustain. Chem. Eng.* **2021**, *9* (21), 7306–7317. https://doi.org/10.1021/acssuschemeng.1c01308.
43. Cházaro-Ruiz, L. F.; Kellenberger, A.; Jähne, E.; Adler, H. J.; Khandelwal, T.; Dunsch, L. In Situ ESR-UV-Vis-NIR Spectroelectrochemical Study of the p-Doping of poly [2-(3-Thienyl)Ethyl Acetate] and Its Hydrolyzed Derivatives. *Phys. Chem. Chem. Phys.* **2009**, *11* (30), 6505–6513. https://doi.org/10.1039/b904529e.
44. Danesh, C. D.; Starkweather, N. S.; Zhang, S. In Situ Study of Dynamic Conformational Transitions of a Water-Soluble Poly(3-Hexylthiophene) Derivative by Surfactant

Complexation. *J. Phys. Chem. B* **2012**, *116* (42), 12887–12894. https://doi.org/10.1021/jp307728r.
45. Su, G.; Yang, C.; Zhu, J. J. Fabrication of Gold Nanorods with Tunable Longitudinal Surface Plasmon Resonance Peaks by Reductive Dopamine. *Langmuir* **2015**, *31* (2), 817–823. https://doi.org/10.1021/la504041f.
46. Dass, A.; Mulik, S.; Sotiriou-Leventis, C.; Leventis, N. Protection of 2-(3-Thienyl)Ethanol with 3-Thienylacetic Acid and Hard Cross-Linked Conducting Films by Electropolymerization of the Ester. *Synth. Met.* **2006**, *156* (14–15), 966–972. https://doi.org/10.1016/j.synthmet.2006.06.015.
47. Ohlan, A.; Singh, K.; Chandra, A.; Dhawan, S. K. Microwave Absorption Behavior of Core?Shell Structured Poly (3,4-Ethylenedioxy Thiophene)?Barium Ferrite Nanocomposites. *ACS Appl. Mater. Interfaces* **2010**, *2* (3), 927–933. https://doi.org/10.1021/am900893d.
48. Futaba, D. N.; Yamada, T.; Kobashi, K.; Yumura, M.; Hata, K. Macroscopic Wall Number Analysis of Single-Walled, Double-Walled, and Few-Walled Carbon Nanotubes by X-Ray Diffraction. *J. Am. Chem. Soc.* **2011**, *133* (15), 5716–5719. https://doi.org/10.1021/ja2005994.
49. Bilger, D.; Sarkar, A.; Danesh, C.; Gopinadhan, M.; Braggin, G.; Figueroa, J.; Pham, T. V.; Chun, D.; Rao, Y.; Osuji, C. O.; Stefik, M.; Zhang, S. Multi-Scale Assembly of Polythiophene-Surfactant Supramolecular Complexes for Charge Transport Anisotropy. *Macromolecules* **2017**, *50* (3), 1047–1055. https://doi.org/10.1021/acs.macromol.6b02416.
50. Kerfoot, J.; Beton, P. H.; Svatek, S. A.; Korolkov, V. V.; Taniguchi, T.; Watanabe, K.; Antolin, E. Fluorescence and Electroluminescence of J-Aggregated Polythiophene Monolayers on Hexagonal Boron Nitride. *ACS Nano* **2020**, *14* (10), 13886–13893. https://doi.org/10.1021/acsnano.0c06280.
51. Sinsinbar, G.; Palaniappan, A.; Yildiz, U. H.; Liedberg, B. A Perspective on Polythiophenes as Conformation Dependent Optical Reporters for Label-Free Bioanalytics. *ACS Sensors* **2022**, *7* (3), 686–703. https://doi.org/10.1021/acssensors.1c02476.
52. Massoumi, B.; Jaymand, M.; Samadi, R.; Entezami, A. A. In Situ Chemical Oxidative Graft Polymerization of Thiophene Derivatives from Multi-Walled Carbon Nanotubes. *J. Polym. Res.* **2014**, *21* (5). https://doi.org/10.1007/s10965-014-0442-3.
53. Sun, C.; Li, X.; Zhao, J.; Cai, Z.; Ge, F. A Freestanding Polypyrrole Hybrid Electrode Supported by Conducting Silk Fabric Coated with PEDOT:PSS and MWCNTs for High-Performance Supercapacitor. *Electrochim. Acta* **2019**, *317*, 42–51. https://doi.org/10.1016/j.electacta.2019.05.124.
54. Welzel, H. P.; Kossmehl, G.; Schneider, J.; Plieth, W. Reactive Groups on Polymer-Covered Electrodes. 2. Functionalized Thiophene Polymers by Electrochemical Polymerization and Their Application as Polymeric Reagents. *Macromolecules* **1995**, *28* (16), 5575–5580. https://doi.org/10.1021/ma00120a023.
55. Oraon, R.; De Adhikari, A.; Tiwari, S. K.; Nayak, G. C. Enhanced Specific Capacitance of Self-Assembled Three-Dimensional Carbon Nanotube/Layered Silicate/Polyaniline Hybrid Sandwiched Nanocomposite for Supercapacitor Applications. *ACS Sustain. Chem. Eng.* **2016**, *4* (3), 1392–1403. https://doi.org/acssuschemeng.5b01389.
56. Jiang, Y.; Liu, J. Definitions of Pseudocapacitive Materials: A Brief Review. *Energy Environ. Mater.* **2019**, *2* (1), 30–37. https://doi.org/10.1002/eem2.12028.
57. Alabadi, A.; Razzaque, S.; Dong, Z.; Wang, W.; Tan, B. Graphene Oxide-Polythiophene Derivative Hybrid Nanosheet for Enhancing Performance of Supercapacitor. *J. Power Sources* **2016**, *306*, 241–247. https://doi.org/10.1016/j.jpowsour.2015.12.028.
58. Parayangattil Jyothibasu, J.; Chen, M. Z.; Lee, R. H. Polypyrrole/Carbon Nanotube Freestanding Electrode with Excellent Electrochemical Properties for High-Performance All-Solid-State Supercapacitors. *ACS Omega* **2020**, *5* (12), 6441–6451. https://doi.org/10.1021/acsomega.9b04029.

59. Parveen, N.; Ansari, M. O.; Cho, M. H. Route to High Surface Area, Mesoporosity of Polyaniline-Titanium Dioxide Nanocomposites via One Pot Synthesis for Energy Storage Applications. *Ind. Eng. Chem. Res.* **2016**, *55* (1), 116–124. https://doi.org/10.1021/acs.iecr.5b02907.
60. Zhu, G.; He, Z.; Chen, J.; Zhao, J.; Feng, X.; Ma, Y.; Fan, Q.; Wang, L.; Huang, W. Highly Conductive Three-Dimensional MnO2-Carbon Nanotube-Graphene-Ni Hybrid Foam as a Binder-Free Supercapacitor Electrode. *Nanoscale* **2014**, *6* (2), 1079–1085. https://doi.org/10.1039/c3nr04495e.